Magnetotransport properties of $Al_xGa_{1-x}N/AlN/GaN$ heterostructures grown on epitaxial lateral overgrown GaN templates

N. Biyikli,[a] X. Ni, Y. Fu, J. Xie, and H. Morkoç
Department of Electrical & Computer Engineering, Virginia Commonwealth University, Richmond, Virginia 23284

H. Cheng and Ç. Kurdak
Department of Physics, University of Michigan, Ann Arbor, Michigan 48109

I. Vurgaftman and J. Meyer
Code 5613, Naval Research Lab, Washington, DC 20375

(Received 22 January 2007; accepted 18 April 2007; published online 13 June 2007)

We studied the low-temperature magnetotransport properties of $Al_xGa_{1-x}N/AlN/GaN$ heterostructures with a two-dimensional electron gas (2DEG). Structures with different Al compositions were grown by metal-organic vapor-phase epitaxy on three types of templates: conventional undoped GaN, *in situ* epitaxial lateral overgrown GaN using a SiN_x nanomask layer, and *ex situ* epitaxial lateral overgrown GaN (ELO-GaN) using a stripe-patterned SiO_2 mask. All of the samples display Shubnikov–de Haas (SdH) oscillations that confirm the existence of 2DEGs. Field-dependent magnetoresistance and Hall measurements further indicate that the overgrown heterostructures have a parallel conducting layer in addition to the 2DEG. To characterize the parallel channel, we repeated the measurements after the 2DEG was etched away. 2DEG carrier density values were then extracted from the SdH data, whereas the zero-field 2DEG conductivity was determined by subtracting the parallel channel conductivity from the total. The quantitative mobility spectrum analysis could not be applied in some cases, due to a large contact resistance between the parallel channels. The resulting 2DEG mobility is about a factor of 2 higher in the ELO-GaN and SiN–GaN samples as compared to the standard control samples. The mobility enhancement is attributed to a reduction of threading dislocations by the two ELO techniques employed. © *2007 American Institute of Physics*. [DOI: 10.1063/1.2745253]

I. INTRODUCTION

Because a two-dimensional electron gas (2DEG) in the $Al_xGa_{1-x}N/GaN$ material system is currently used in high-power field effect transistors for microwave applications, the transport properties of such structures are of considerable interest.[1,2] While the device performance has steadily improved as a result of better quality templates and optimized growth conditions,[3–8] further progress will depend on understanding and minimizing the crystal defects. A primary figure of merit for defect-reduction studies is the low-temperature AlGaN/GaN 2DEG mobility, which is limited mainly by the high density of threading dislocations generated at the lattice-mismatched GaN/Al_2O_3 interface. Fewer defects would reduce the scattering associated with threading dislocations and other mechanisms that are effective in the low-density regime.[9,10]

There are two main methods for defect reduction in epitaxial GaN layers. One is to use a low-dislocation-density template such as native GaN or thick, freestanding hydride phase vapor epitaxy (HVPE)-grown GaN.[11] The subsequent 2DEG layers grown on such substrates emulate the low-extended-defect pattern and result in high-mobility 2DEG layers.[6,7] The other method employs growth on lattice-mismatched sapphire substrates, but attempts to filter the threading dislocations by utilizing defect-blocking mask layers. This method relies on epitaxial lateral overgrowth (ELO), commencing from the nearly defect-free GaN facets,[12] to laterally overgrow epilayers with lower dislocation densities. The weakness of this method is that threading dislocations extend along the unmasked (window) areas where GaN grows vertically and new defects are also introduced at the coalescence boundaries. Successful masking techniques for ELO have included porous SiN_x (Ref. 13–17) or TiN (Ref. 18) layers, as well as the more conventional *ex situ* deposited SiN_x or SiO_2 striped mask templates.[19–24] Among them, porous SiN_x mask layers have the advantage of *in situ* growth, without any requirement for further processing outside the growth chamber.

The present work seeks to improve the electron mobility in $Al_xGa_{1-x}N/AlN/GaN$ heterostructures grown by metal-organic vapor-phase epitaxy (MOVPE), by comparing two ELO techniques that employ *in situ* grown porous SiN_x and *ex situ* grown striped SiO_2 as the defect-blocking mask layers. We discuss low-temperature magnetotransport measurements and analyze the influence of template quality on the $Al_xGa_{1-x}N/AlN/GaN$ transport properties. A significant enhancement of the 2DEG mobility is observed in the samples grown on low-dislocation-density GaN templates.

II. EXPERIMENTAL DETAILS

The $Al_xGa_{1-x}N/AlN/GaN$ heterostructures were grown in a custom rotating-disk low-pressure MOVPE system with

[a]Electronic mail: nbiyikli@vcu.edu

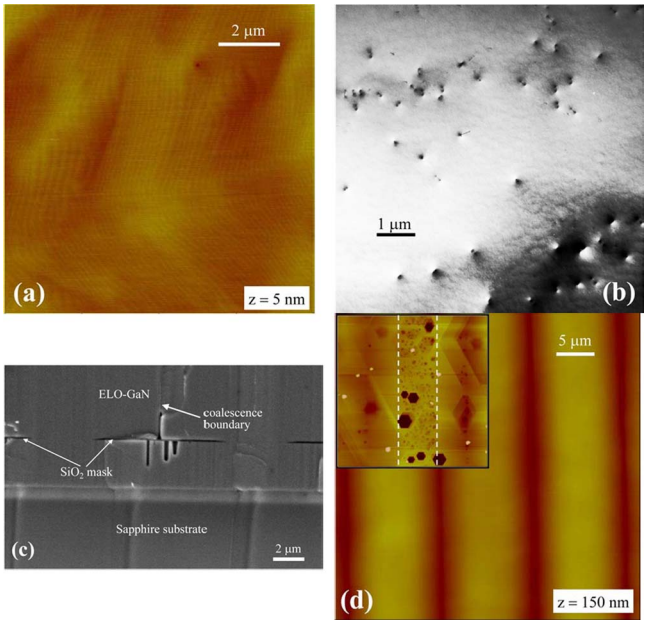

FIG. 1. (Color online) (a) 10×10 μm^2 AFM scan of the SiN–GaN template surface showing smooth surface and clear atomic steps. (b) Plan-view TEM picture of the SiN–GaN template reveals that the threading dislocations are about 9×10^7 cm^{-2}. (c) Cross-sectional SEM picture of the ELO-GaN template, showing the SiO_2 mask and ELO-GaN coalescence boundary. (d) 40×40 μm^2 AFM scan of the ELO-GaN template, where the dark lines correspond to the coalescence boundaries. The inset shows a 20×20 μm^2 scan of the same template after a 2 min KOH etch for the etch-pit study. The window area is marked within the dashed lines.

a vertical chamber. Ammonia (NH_3), trimethylgallium (TMGa), and trimethylaluminum (TMAl) were used as the precursors for nitrogen, gallium, and aluminum, respectively. Hydrogen was used as the carrier gas, and the growth was accomplished under high-speed rotation (~500 rpm). The growth on *c*-plane (0001) sapphire substrates was initiated with a 25-nm-thick low-temperature (~550 °C) GaN nucleation layer. A 3-μ-thick undoped GaN epilayer was then grown at 1000 °C under 200 mTorr, using a V/III ratio of 4000 and average growth rate of ~1.6 μm/h. This *u*-GaN template served as a basis template for all samples. The x-ray diffraction (XRD) measurements of the base template yielded (002) and (102) peak full width at half maximum (FWHM) values of ~8 and ~5.5 arc min, respectively. Atomic force microscopy (AFM) scans and etch-pit studies showed that the basis template had a threading dislocation density in the low 10^9 cm^{-2} range.

The SiN–GaN template was grown *in situ* by ELO. On top of the *u*-GaN epilayer, a porous SiN_x layer was grown at 1020 °C and 200 mTorr, by flowing 50 SCCM (SCCM denotes cubic centimeter per minute at STP) of 100 ppm silane diluted in hydrogen for 5.5 min. The nominal thickness of this porous SiN_x layer was ≈2 nm. Subsequently, lateral overgrowth was initiated from the GaN openings in the pores of the SiN_x nanomask. ELO was performed at 1040 °C under a reduced reactor pressure (76 mTorr) and V/III ratio (2000) to increase the lateral overgrowth rate. After 3 h of overgrowth, complete coalescence was achieved. Figure 1(a) shows clear atomic steps in a 10×10 μm^2 AFM scan of the SiN–GaN template surface. XRD rocking curve exhibited (002) and (102) peaks with FWHM of 3.6 and 3.4 arc min respectively, indicating a significant reduction in threading dislocations as well as most likely point defects. The plan-view and cross-sectional transmission electron microscopy (TEM) measurements in similar samples also demonstrated the effectiveness of the SiN_x nanomask layer in reducing threading dislocations.[25] A plan-view TEM image is shown in Fig. 1(b), where the SiN_x nanomask layer effectively blocks the threading dislocations from penetrating into the upper ELO-GaN layer.[25] The average threading dislocation density in the SiN–GaN template is determined as $\sim9\times10^7$ cm^{-2} from the TEM study. A similar density of threading dislocations was found from an etch-pit study, in which a piece of SiN–GaN template was etched for about 2 min in molten KOH solution and the resulting hexagonal etch pits counted with AFM.

For the *ex situ* ELO–GaN template, the base template was coated with ~150 nm of SiO_2 in an ultrahigh-vacuum chemical vapor deposition (UHV-CVD) system. Using standard lithography and etching techniques, a set of parallel 10-μm-wide SiO_2 mask stripes separated by 4-μm-wide window areas was formed in the SiO_2 mask layer. The stripe pattern was aligned along the $\langle1\bar{1}00\rangle$ direction (*m* direction) for the lateral growth to take place along the $\langle11\bar{2}0\rangle$ direction (*a* direction) that maximizes the lateral growth rate.[12] The sample was then loaded into the MOVPE reactor and ELO was commenced in the 4-μm-wide GaN window areas without any nucleation on the dielectric mask. 3 h of ELO at 1040 °C, 30 mTorr, and V/III ratio of 2000 were sufficient to obtain a completely coalesced surface. The lateral-to-vertical growth rate was optimized at a ratio of 3:1 such that within 2 h of overgrowth the GaN wings met at the coalescence boundary. Additional deposition following the coalescence served to smooth the sample surface, which is critical for high 2DEG mobility. Figure 1(c) shows a cross-sectional scanning electron microscopy (SEM) image of the completed ELO-GaN template. In the 40×40 μm^2 AFM illustration of the surface morphology shown in Fig. 1(d), the dark regions correspond to the coalescence boundary where a ~50–70 nm dip is observed. The window region, where the GaN overgrowth is vertical, is at the center of the brighter areas. The density of threading dislocations in the ELO-GaN template was estimated from an etch-pit study. The inset in Fig. 1(d) shows a 20×20 μm^2 AFM image scanned after a 2 min KOH etch. The highly defective window area (marked with dashed lines) is easily differentiated from the low-dislocation wing area. Along the window stripes, the vertically overgrown GaN allows most of the threading dislocations to propagate from the substrate to the upper surface. Counting the pits yields an average dislocation density of $\sim6\times10^8$ cm^{-2} in the window areas. Dislocations were significantly reduced in the wing areas, with most located at the coalescence boundaries where two overgrowing GaN wings meet. The ~4 μm stripes between the windows and coalescence boundaries contain very few dislocations. The average density in the wing regions is estimated as $\sim1\times10^7$ cm^{-2}. The overall average threading dislocation density in the ELO-GaN template is projected to be $\sim2\times10^8$ cm^{-2}.

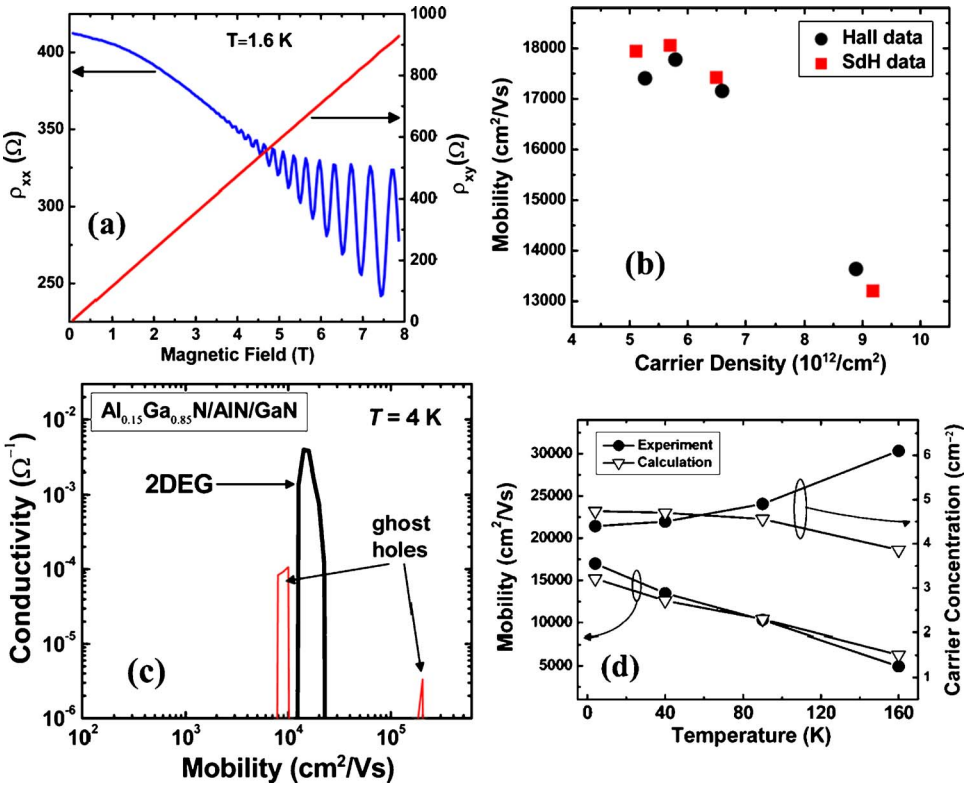

FIG. 2. (Color online) (a) Longitudinal and Hall resistivity curves measured at 1.6 K for the $Al_{0.30}Ga_{0.70}N/AlN/GaN$ reference sample. (b) Density-dependent 2DEG mobility of the illuminated $Al_{0.30}Ga_{0.70}N/AlN/GaN$ sample determined by both SdH and Hall data. (c) Mobility spectrum calculated by QMSA for the $Al_{0.15}Ga_{0.85}N/AlN/GaN$ reference sample at $T=4$ K. (d) Temperature-dependent carrier density and mobility curves determined from the raw experimental data and QMSA.

$Al_xGa_{1-x}N$ layers were grown on top of the aforementioned templates to form the 2DEG systems. Each heterostructure comprised an additional ~1 μm GaN layer, a ~1-nm-thick AlN interfacial layer, a ~25 nm $Al_xGa_{1-x}N$ layer, and a ~3 nm GaN cap layer, all nominally undoped. The 2DEG channel forms as a result of spontaneous and piezoelectric polarization effects at the GaN/AlN heterointerface. The AlN interfacial layer is inserted to minimize penetration of the 2DEG wave functions into the $Al_xGa_{1-x}N$ layer, thereby reducing the scattering by alloy disorder.[26–28] The heterostructure layers were grown at 1060 °C under 30 mTorr, using a V/III ratio of ~600. The Al concentration varied from 10% to 30% in the reference samples, whereas 20% was used for the SiN–GaN and ELO-GaN samples. Six-contact Hall bars were prepared, with Ohmic contacts formed using Ti/Al/Ti/Au (30 nm/100 nm/30 nm/50 nm) alloyed at 900 °C for 1 min.

Magnetic field-dependent longitudinal resistance (ρ_{xx}) and transverse (Hall) resistance (ρ_{xy}) measurements were carried out at $T=1.6$ K in a variable temperature liquid-He cryostat equipped with an 8 T superconducting magnet. A low-noise *ac* lock-in technique was used with a low-noise current preamplifier to record the sample voltages. To avoid sample heating, a low excitation current of 1 μA was used. The data analysis was used to determine carrier densities and mobilities in the 2DEG samples.

III. RESULTS

A. Reference samples

$Al_xGa_{1-x}N/AlN/GaN$ samples grown on conventional *u*-GaN templates with $x=0.10$, 0.15, 0.25, and 0.30 served as references to compare with the 2DEG structures grown on SiN–GaN and ELO–GaN templates. Every sample showed clear single-period Shubnikov–de Haas (SdH) oscillations in its magnetoresistance, confirming the existence of a 2DEG at the AlN/GaN interface. Figure 2(a) shows the longitudinal (ρ_{xx}) and Hall (ρ_{xy}) resistivities versus magnetic field (B) for the $Al_{0.30}Ga_{0.70}N/AlN/GaN$ sample at $T=1.6$ K. The ρ_{xx} curve displays strong SdH oscillations commencing around 3 T, whereas the ρ_{xy} curve increases linearly with magnetic field as expected. The corresponding 2DEG carrier density was determined by two methods. While for an ideal 2DEG system the slope of $\rho_{xy}(B)$ is proportional to $1/n_{2DEG}$, one can alternatively extract the 2DEG carrier density from the period of the SdH oscillations. Using persistent photoconductivity (PPC) under optical illumination[29] to alter (increase) the sample's carrier density, we have determined the carrier density and mobility of the same $Al_{0.30}Ga_{0.70}N/AlN/GaN$ sample by both methods and plotted the results in Fig. 2(b). Illumination increased the carrier density from 5.2×10^{12} to 9.0×10^{12} cm^{-2}. The corresponding electron mobility showed a slight increase up to $n=5.7\times10^{12}$ cm^{-2}, where $\mu=17\,900$ cm^2/V s, and decreased thereafter. The figure shows that the carrier densities and mobilities obtained by the two methods agree well for this sample, indicating that the 2DEG is of reasonable quality and no significant parallel conducting channels are present. Similar results were obtained for the other reference 2DEG samples with different Al compositions. By varying the Al content in the barrier layer from 10% to 30% and also using the PPC effect, we were able to change the carrier density from 5×10^{11} to 1×10^{13} cm^{-2}. All of the mobilities tended to increase with the carrier density initially, before saturating

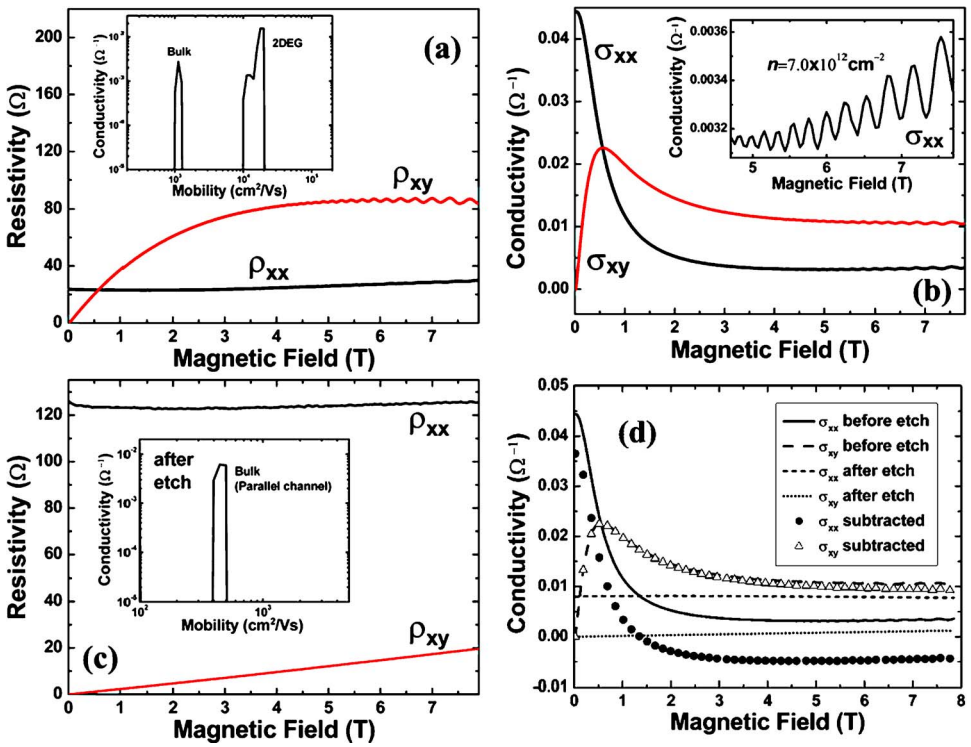

FIG. 3. (Color online) (a) Longitudinal and Hall resistivities measured at 1.6 K for the $Al_{0.20}Ga_{0.80}N/AlN/GaN$ sample grown on the SiN–GaN template. The inset shows the QMSA mobility spectrum for this sample. (b) Corresponding longitudinal and Hall conductivities, with magnified SdH oscillations in the inset. (c) Measured resistivities after the recess etch. Inset shows the corresponding QMSA spectrum. (d) Conductivity curves before and after the recess etch, also showing the implied 2DEG conductivities obtained following subtraction.

at $\approx 6\times10^{12}$ cm^{-2} and decreased at higher n. The peak mobility for the illuminated $Al_{0.15}Ga_{0.85}N/AlN/GaN$ sample exceeded 20 000 cm^2/V s.

The quantitative mobility spectrum analysis (QMSA) is an effective technique for treating mixed conduction by multiple carrier species in a semiconductor, since it simultaneously extracts the densities and mobilities for each class of electron and hole.[30–32] The experimental inputs to this analysis are the variable-field longitudinal and Hall resistivity data. Figure 2(c) shows QMSA results for the $Al_{0.15}Ga_{0.85}N/AlN/GaN$ sample measured at 4 K (similar results were obtained for the other reference samples with different Al concentrations). The dominant feature in the figure is a high-mobility electron corresponding to the 2DEG channel. This is accompanied by unphysical "ghost holes" with much lower apparent densities, artifacts of a type that are seen frequently in mobility spectrum analyses.[31] The carrier density and mobility derived from QMSA are 4.7×10^{12} cm^{-2} and 15 200 cm^2/V s, respectively, which are close to the values of 4.4×10^{12} cm^{-2} and 16 900 cm^2/V s obtained from the raw experimental data. This close agreement again indicates that no significant parallel conduction exists in the reference samples. Figure 2(d) shows that up to temperatures as high as 90 K, the carrier densities and mobilities derived from the raw data agree well with those from QMSA. At higher temperatures the QMSA carrier density deviates from the raw result, indicating that bulk electrons which were frozen out at low temperatures begin to contribute to the conductivity. For example, at $T=160$ K a lower-mobility peak corresponding to the bulk three-dimensional (3D) electron within the u-GaN template appears in the QMSA spectrum.

B. Porous SiN–GaN sample

The $Al_{0.20}Ga_{0.80}N/AlN/GaN$ sample grown on the SiN–GaN template showed different magnetotransport characteristics from those grown on the conventional templates. That the Hall data are nonlinear in the ρ_{xx} and ρ_{xy} plots of Fig. 3(a) for $T=1.6$ K indicates the presence of multiple conducting channels. The parallel channel is confirmed by the corresponding QMSA spectrum shown as the inset to Fig. 3(a). Besides the high-mobility carrier associated with the 2DEG, a lower-mobility electron also appears due to bulk electrons in the parallel channel. The derived 2DEG carrier density and mobility values are 1.4×10^{13} cm^{-2} and 18 000 cm^2/V s, respectively, while those for the bulk electron are 3.1×10^{14} cm^{-2} and 1100 cm^2/V s. Note that the 2DEG carrier density extracted from QMSA is significantly larger than that in the control samples.

It should be cautioned that because the bulk channel lies far below (~5 μm) the 2DEG channel, the usual assumption in mixed-conduction analyses of negligible contact resistance *between* the channels may not hold here. We expect the Hall bar's annealed Ohmic metal contacts to extend only to the vicinity of the 2DEG layer, causing the contact resistance to the bulk channel to be rather large (about 10^2–10^3 Ω). As a result, the bulk channel's conduction contribution is suppressed relative to that of the 2DEG.

To address this problem we have designed the following experiment: by recess etching the top $Al_{0.20}Ga_{0.80}N/AlN$ layers we first removed the 2DEG and then repeated the magnetotransport measurements on the recess-etched samples containing the bulk channel only. Having two sets of data in hand, we then converted the resistivities into conductivity tensor elements using the following relations:

$$\sigma_{xx} = \frac{\rho_{xx}}{\rho_{xx}^2 + \rho_{xy}^2}, \tag{1}$$

$$\sigma_{xy} = \frac{\rho_{xy}}{\rho_{xx}^2 + \rho_{xy}^2}. \tag{2}$$

If the contact resistances to the 2DEG and bulk channels are both negligible, the 2DEG conductivity can be extracted by subtracting the bulk conductivity from the total conductivity,

$$\sigma_{xx}^{2DEG}(B) = \sigma_{xx}^{Total}(B) - \sigma_{xx}^{Bulk}(B). \tag{3}$$

Using the zero-field conductivity value, the 2DEG mobility can be determined if its carrier density is known. Fortunately, the SdH oscillations observed in the longitudinal resistivity for this sample provide an independent determination of the 2DEG carrier density. Figure 3(b) plots the conductivity curves before the recess etch, while the inset magnifies the SdH oscillations. The derived 2DEG carrier density is 7.0×10^{12} cm^{-2}. After recess etching $\sim$100 nm from the top using BCl_3-plasma reactive ion etching, we again measured the field-dependent resistivities. Several differences are observed in the resulting data shown in Fig. 3(c): the SdH oscillations disappear and the Hall resistance becomes linear, confirming that the 2DEG is completely removed. From the Hall data we find that the bulk channel carrier density is 2.5×10^{14} cm^{-2}, yielding a mobility of 200 cm^2/V s. The QMSA result for the recess-etched sample is shown as the inset to Fig. 3(c). The spectrum contains only a single electron corresponding to bulk conduction within the SiN–GaN template, with 470 cm^2/V s mobility and 4.2×10^{14} cm^{-2} carrier density. Figure 3(d) shows the nominal extraction of the 2DEG conductivities from the data sets measured before and after the recess etch. Because of the contact resistance issue, however, the 2DEG conductivity extracted in this manner should be viewed only as a lower bound on the actual value. The problem is most pronounced at higher magnetic fields ($B>1.3$ T) where the implied σ_{xx} becomes unphysically negative. To confirm the possible effects of a large contact resistance to the bulk channel, we modeled the Hall bar as a two-layer structure with a finite contact resistance in between. Using the experimental resistivity and carrier density values, this model yields a negative apparent conductivity for $B>0.9$ T that is consistent with our experimental result.

We can also obtain an upper bound on the 2DEG conductivity by considering the extreme case where there is no bulk contribution and only the 2DEG contributes to the total. Since the true conductivity is between these two boundaries, we conclude that the 2DEG mobility must fall in the range of 32 400–39 400 cm^2/V s. Even though the true value is probably closer to the lower bound, that nonetheless represents a 60% enhancement over the 2DEG mobility in the reference sample with similar carrier density.

When we compare the parallel conduction results, the mobility and carrier density are in reasonable agreement. While we know from the reference sample data that the bulk electrons in *u*-GaN freeze out at low temperatures, the observation of a high electron density at 1.6 K suggests that the parallel conduction is due to the presence of the SiN_x layer.

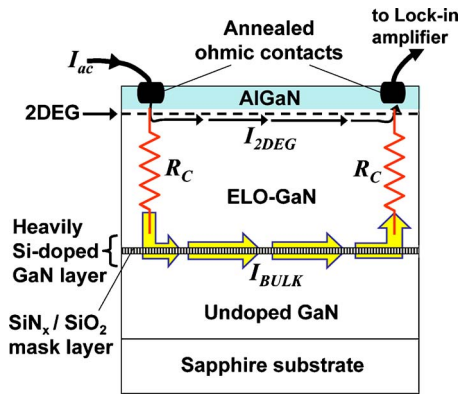

FIG. 4. (Color online) Schematical representation of the multicarrier conduction in the AlGaN/AlN/GaN heterostructures grown on *in situ* and *ex situ* ELO-GaN templates. The contact resistance to the parasitic bulk channel is shown by R_C.

The porous SiN_x may supply a sufficient density of Si atoms to the bottom face of the overgrown GaN epilayer to induce the formation of a degenerate impurity band. Such a degenerately Si-doped GaN layer at the GaN/SiN_x interface would not be expected to exhibit carrier freeze out. A schematic of the multi channel conduction within the 2DEG/SiN–GaN samples is shown in Fig. 4, where R_C represents the unknown contact resistance to the parallel bulk conduction channel located around the heavily Si-doped GaN/SiN_x interface. A similar mechanism is also valid for parallel conduction in 2DEG/ELO-GaN samples as will be explained hereafter.

C. ELO-GaN samples

Two Hall bars were fabricated from the $Al_{0.20}Ga_{0.80}N$/AlN/GaN sample grown on the ELO-GaN template. One was aligned to be parallel to the SiO_2 stripes (parallel sample), whereas in the other the SiO_2 stripes were perpendicularly aligned (perpendicular sample). Our aim was to investigate the orientation dependence of 2DEG electron transport on an ELO-GaN template. As in the case of the SiN–GaN sample, measurements were carried out at 1.6 K, before and after the recess etch. A similar contact resistance issue for the parallel channel made the use of QMSA invalid.

Figure 5(a) shows the longitudinal and Hall resistivities measured for the parallel Hall bar sample before and after the recess etch. In Fig. 5(b), the ρ_{xx} dependence on magnetic field is shown as a function of sample illumination. The magnified plot in the inset illustrates that the SdH oscillations became stronger after the sample was illuminated. The PPC effect enhanced the 2DEG conduction due to an increase of the carrier density from 4.7×10^{12} to 7.3×10^{12} cm^{-2}.

As for the SiN–GaN sample discussed above, we estimated the electron mobility by comparing the resistivities before and after removal of the 2DEG. The data obtained after the recess etch showed the ELO-GaN template to have a bulk electron density of 7.1×10^{13} cm^{-2} and mobility of 1550 cm^2/V s. Although the density is not as high as in the SiN–GaN sample, a parallel channel is found to exist in the ELO-GaN sample as well. The source for the parallel conduction in ELO-GaN samples can be attributed to the SiO_2

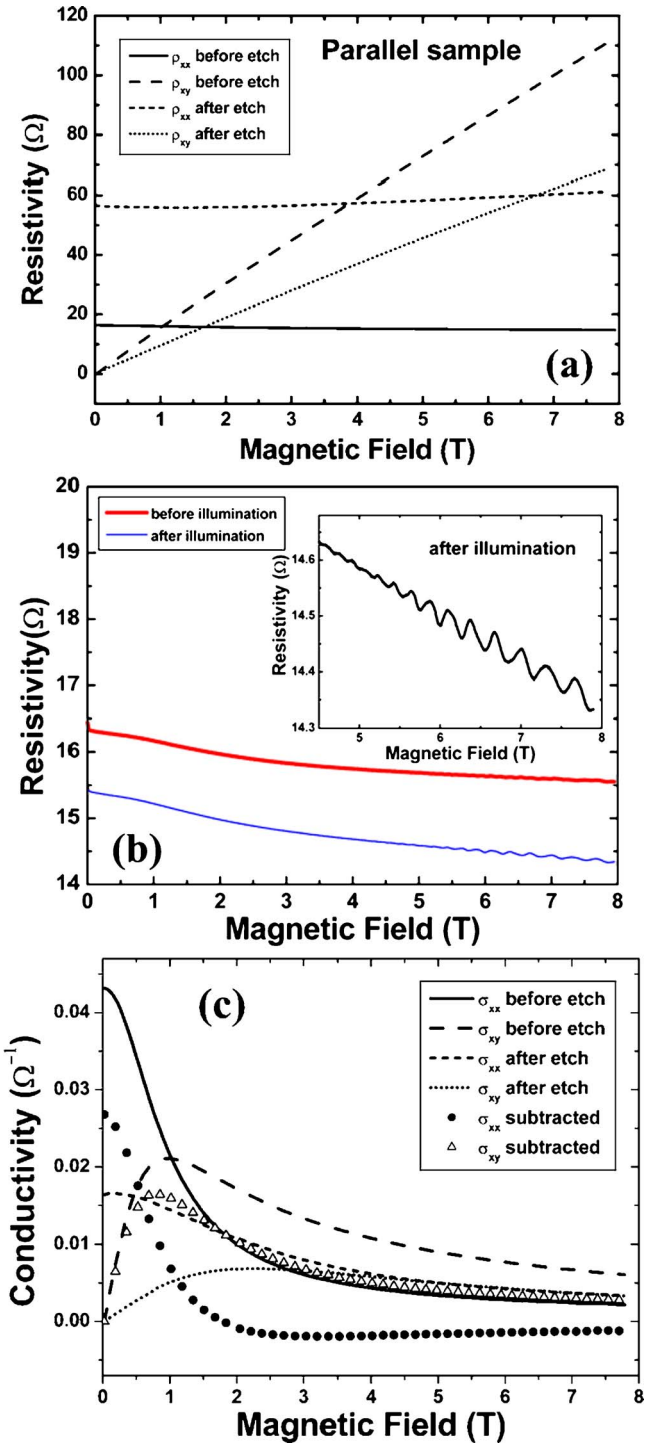

FIG. 5. (Color online) (a) Experimental longitudinal and Hall resistivities at 1.6 K for the parallel Hall-bar $Al_{0.20}Ga_{0.80}N/AlN/GaN$ sample grown on the ELO-GaN template before and after the recess etch. (b) $\rho_{xx}(B)$ for the same sample before and after illumination. The inset magnifies the SdH oscillations. (c) Longitudinal and Hall conductivities for the same sample before and after the recess etch, along with the subtracted dependences.

mask layer used (Fig. 4). As in the case of the SiN-ELO samples, the diffusion of Si atoms into the ELO-GaN probably formed a degenerately doped layer whose electrons do not freeze out at low temperatures. The experimental longitudinal and Hall conductivity curves, along with the implied 2DEG contributions obtained by subtracting the bulk conductivities from the totals, are plotted in Figure 5(c). As was found above for the SiN–GaN sample, the implied 2DEG conductivity becomes unphysically negative for $B>1$ T, which may again be attributed to errors associated with the unknown contact resistance between the two parallel channels. From the subtracted zero-field conductivity, a lower bound of 34 800 cm^2/V s is obtained for the 2DEG mobility in the illuminated sample. The upper bound based on the preetch conductivity is 50 000 cm^2/V s.

Magnetoresistance data at 1.6 K for the perpendicular ELO-GaN sample, before and after the recess etch, are shown in Fig. 6(a). The clear single-period SdH oscillations that are observed before etching disappear after removal of 2DEG. Figure 6(b) illustrates the effects of illumination on $\rho_{xx}(B)$. PPC increased the carrier density from 4.2×10^{12} to 5.2×10^{12} cm^{-2}, and the SdH oscillations gained strength. Figure 6(c) shows the corresponding conductivity data before and after the etch, along with the subtracted difference curves. The implied lower bounds on the 2DEG mobility are 39 400 and 40 700 cm^2/V s for the cases of before and after illumination, respectively. This lower bound represents more than a twofold enhancement with respect to the reference 2DEG samples. The upper limits on the 2DEG mobilities, obtained from the total preetch conductivity data, are 63 500 and 65 600 cm^2/V s for before and after illumination, respectively. The bulk channel exhibited an electron density of 3.3×10^{13} cm^{-2} and mobility of 3120 cm^2/V s. We note that the ELO-GaN samples exhibit an orientation dependence, with the perpendicular sample having a smaller electron density and higher mobility than the parallel sample.

IV. DISCUSSION

Figure 7 summarizes the results of our study, encompassing the 2DEG mobilities and carrier densities (with and without illumination) for the reference, SiN–GaN, and ELO-GaN samples at $T=1.6$ K. In the case of the SiN–GaN and ELO-GaN samples, the values shown are lower bounds, as they represent conservative estimates of the true 2DEG mobilities. It is evident lateral overgrowth substantially improved the 2DEG mobility, with both *in situ* grown SiN_x and *ex situ* grown SiO_2 masking layers effectively blocking the threading dislocations. Both mobilities are clearly enhanced by around a factor of 2 or higher; although the exact values could not be determined because of the unknown contact resistances to the parallel bulk channels. For the same reason, a direct quantitative comparison between growth on the SiN–GaN and ELO-GaN templates is not meaningful at this point.

The 2DEG samples grown on conventional *u*-GaN templates displayed electron mobilities up to 20 000 cm^2/V s. PPC extended the 2DEG carrier density range from 5×10^{11} to 1.1×10^{13} cm^{-2}, with the mobility peaking around $n\approx6\times10^{12}$ cm^{-2}. However, PPC was not as effective in any of the lateral overgrowth samples, probably due to the substantial parallel bulk conduction. In that case we should expect the mobility to increase toward lower carrier densities and peak in the low 10^{12} cm^{-2} range, due to the reduced

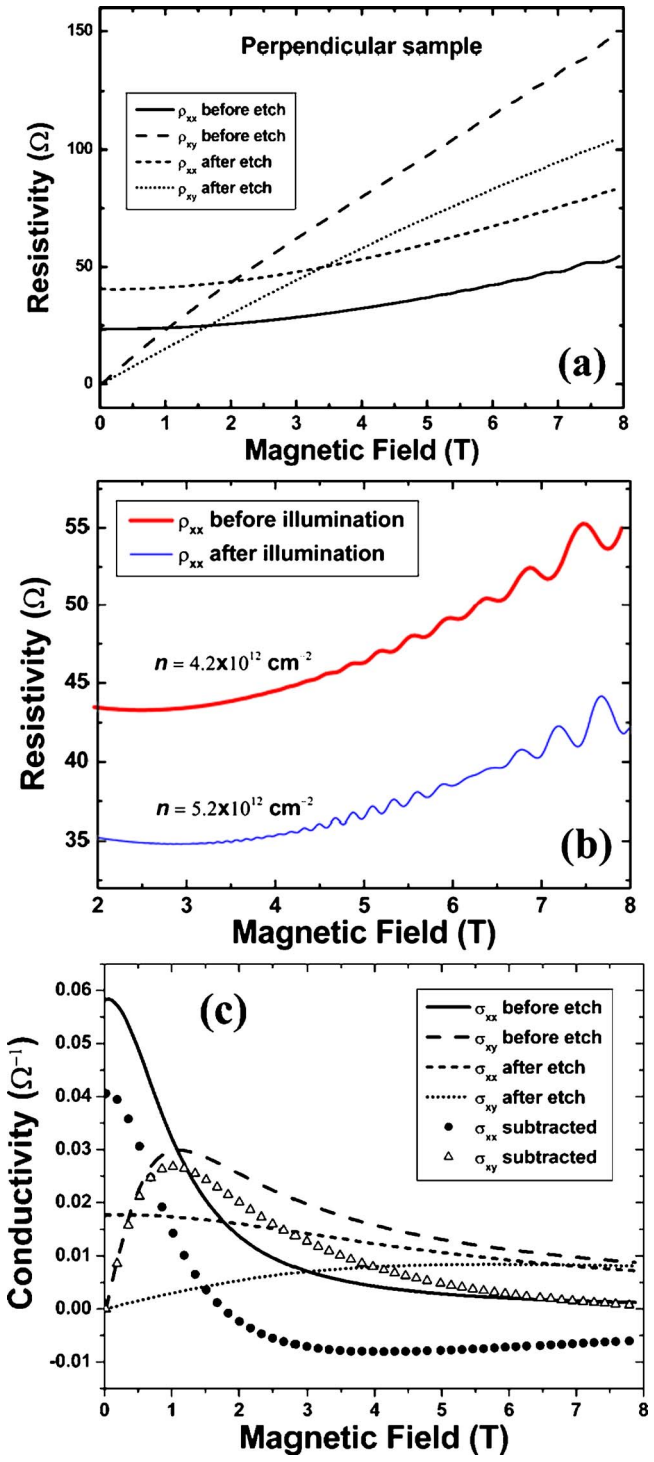

FIG. 6. (Color online) (a) Measured longitudinal and Hall resistivities at 1.6 K for the perpendicular Hall-bar $Al_{0.20}Ga_{0.80}N/AlN/GaN$ sample grown on the ELO-GaN template before and after the recess etch. (b) $\rho_{xx}(B)$ for the same sample before and after illumination. (c) Longitudinal and Hall conductivities for the same sample before and after the recess etch, along with the subtracted dependences.

scattering by charged dislocations.[3] The samples on laterally overgrown GaN templates showed lower-bound 2DEG mobilities exceeding 40 000 cm^2/V s.

One approach to determining the true 2DEG mobility in a sample with multiple conducting channels separated by a large contact resistance would be to isolate the parallel bulk channel experimentally. This could be realized by growing a

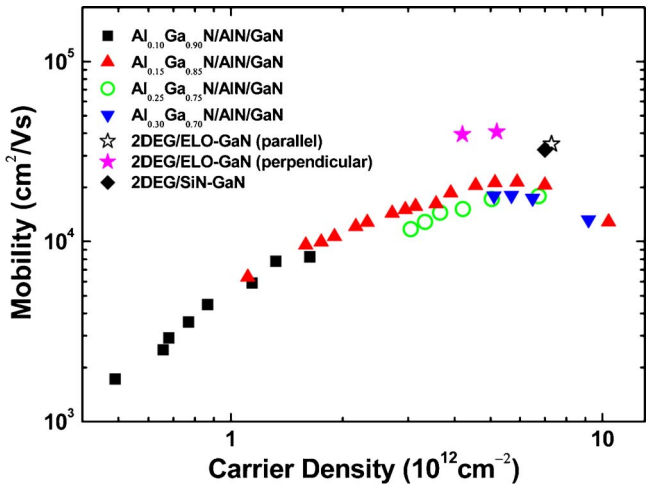

FIG. 7. (Color online) Summary of 2DEG mobilities vs carrier density for $Al_xGa_{1-x}N/AlN/GaN$ 2DEG samples grown on conventional *u*-GaN (reference), SiN–GaN, and ELO-GaN templates. All measurements are at 1.6 K.

p-type Mg-doped GaN layer between the 2DEG and the SiN_x or SiO_2 layer. Fe doping may also be effective, since Fe:GaN is known to be semi-insulating, but segregation issues would have to be addressed. However, in either case the additional Mg or Fe impurities could potentially degrade the quality of subsequent layers by forming new defects in the overgrown GaN. A second approach would be to form the contacts in such a way that there is similarly low resistance to all of the conducting channels. Experiments to solve this problem are currently ongoing.

In summary, we have demonstrated that MOVPE-grown SiN–GaN and ELO-GaN templates are promising substrates for high-quality $Al_xGa_{1-x}N/AlN/GaN$ 2DEG structures. Both ELO techniques effectively reduce the threading dislocation density in the overgrown layers. Electron mobilities within lower and upper-bound limits of 32 400–39 400 and 40 700–65 600 cm^2/V s were determined for 2DEG samples grown on SiN–GaN and ELO-GaN templates, respectively.

ACKNOWLEDGMENTS

The work at VCU was supported by the Air Force Office of Scientific Research under the direction of Dr. K. Reinhardt and the work at UM was supported by the NSF through Grant No. DMR-0606039. The laboratory at VCU benefited from grants from the Office of Naval Research and the National Science Foundation, and equipment funds provided by Virginia Commonwealth University. The authors would like to thank the MOVPE colleagues Y. Fu and X. Ni for useful discussions and maintenance of the system, and Professor T. S. Kuan for our ongoing collaborations on the general issue of defect reduction using porous templates.

[1]H. Morkoç, *Handbook of Nitride Semiconductors and Devices*, 1st ed. (Springer, Berlin, 2007).
[2]S. N. Mohammad, A. Salvador, and H. Morkoç, Proc. IEEE **83**, 1420 (1996).
[3]M. J. Manfra, L. N. Pfeiffer, K. W. West, H. L. Stormer, K. W. Baldwin, J. W. P. Hsu, and R. J. Molnar, Appl. Phys. Lett. **77**, 2888 (2000).
[4]L. McCarthy *et al.*, Appl. Phys. Lett. **78**, 2235 (2001).
[5]I. P. Smorchkova *et al.*, J. Appl. Phys. **90**, 5196 (2001).
[6]M. J. Manfra, K. W. Baldwin, A. M. Sergent, K. W. West, R. J. Molnar,

and J. Caissie, Appl. Phys. Lett. **85**, 5394 (2004).
[7]C. Skierbiszewski *et al.*, Appl. Phys. Lett. **86**, 102106 (2005).
[8]S. Schmult, M. J. Manfra, A. M. Sergent, A. Punnoose, H. T. Chou, D. Goldhaber-Gordon, and R. J. Molnar, Phys. Status Solidi B **243**, 1706 (2006).
[9]D. Jena, I. Smorchkova, A. C. Gossard, and U. K. Mishra, Phys. Status Solidi B **228**, 617 (2001).
[10]L. Hsu and W. Walukiewicz, Appl. Phys. Lett. **80**, 2508 (2002).
[11]D. Huang *et al.*, Solid-State Electron. **45**, 711 (2001).
[12]P. Gibart, Rep. Prog. Phys. **67**, 667 (2004).
[13]S. Sakai, T. Wang, Y. Morishima, and Y. Naoi, J. Cryst. Growth **221**, 334 (2000).
[14]A. Dadgar *et al.*, Appl. Phys. Lett. **82**, 28 (2003).
[15]X. L. Fang, Y. Q. Wang, H. Meidia, and S. Mahajan, Appl. Phys. Lett. **84**, 484 (2004).
[16]A. Sagar, R. M. Feenstra, C. K. Inoki, T. S. Kuan, Y. Fu, Y. T. Moon, F. Yun, and H. Morkoç, Phys. Status Solidi A **202**, 772 (2005).
[17]K. Pakua, R. Bozÿek, J. M. Baranowski, J. Jasinski, and Z. Lilienthal-Weber, J. Cryst. Growth **267**, 1 (2004).
[18]Y. Fu *et al.*, J. Appl. Phys. **99**, 033518 (2006).
[19]O. H. Nam, M. D. Bremser, T. S. Zheleva, and R. F. Davis, Appl. Phys. Lett. **71**, 2638 (1997).
[20]S. Haffouz, H. Lahreche, P. Vennegues, B. Beaumont, F. Omnes, and P. Gibart, Appl. Phys. Lett. **73**, 1278 (1998).
[21]T. Akasaka, Y. Kobayashi, S. Ando, and N. Kobayashi, Appl. Phys. Lett. **71**, 2196 (1997).
[22]B. Beaumont *et al.*, Phys. Status Solidi A **176**, 567 (1999).
[23]K. Hiramatsu *et al.*, J. Cryst. Growth **221**, 316 (2000).
[24]I. Kidoguchi, A. Ishibashi, G. Sugahara, and Y. Ban, Appl. Phys. Lett. **76**, 3768 (2000).
[25]J. Xie, Ü. Özgür, Y. Fu, X. Ni, H. Morkoç, C. K. Inoki, T. S. Kuan, J. V. Foreman, and H. O. Everitt, Appl. Phys. Lett. **90**, 041107 (2007).
[26]L. Shen *et al.*, IEEE Electron Device Lett. **22**, 457 (2001).
[27]M. Miyoshi, H. Ishikawa, T. Egawa, K. Asai, M. Mouri, T. Shibata, M. Tanaka, and O. Oda, Appl. Phys. Lett. **85**, 1710 (2004).
[28]L. Hsu and W. Walukiewicz, J. Appl. Phys. **89**, 1783 (2001).
[29]N. Biyikli, Ü. Özgür, X. Ni, Y. Fu, H. Morkoç, and Ç. Kurdak, J. Appl. Phys. **100**, 103702 (2006).
[30]J. R. Meyer, C. A. Hoffman, F. J. Bartoli, D. A. Arnold, S. Sivananthan, and J. P. Faurie, Semicond. Sci. Technol. **8**, 805 (1993).
[31]I. Vurgaftman, J. R. Meyer, C. A. Hoffman, D. Redfern, J. Antoszewski, L. Farone, and J. R. Lindemuth, J. Appl. Phys. **84**, 4966 (1998).
[32]A. Saxler *et al.*, J. Appl. Phys. **87**, 369 (2000).